KAPL-P-000071
(K-98042)

ANNULAR FLOW OF R-134A THROUGH A HIGH ASPECT RATIO DUCT; LOCAL VOID FRACTION, DROPLET VELOCITY AND DROPLET SIZE MEASUREMENTS

TA Trabold, R Kumar, PF Vassallo

CONF-981107--

November 15-10, 1998

NOTICE

KAPL ATOMIC POWER LABORATORY SCHENECTADY, NEW YORK 12301

Operated for the U. S. Department of Energy
by KAPL, Inc. a Lockheed Martin company

Annular Flow of R-134a in a Vertical Duct: Local Void Fraction, Droplet Velocity and Droplet Size Measurements

T.A. Trabold, R. Kumar and P.F. Vassallo
Lockheed Martin Corporation
Schenectady, NY 12309

Abstract

Local measurements were made in annular flow of R-134a through a vertical duct. Using a gamma densitometer, hot-film anemometer and laser Doppler velocimeter, profiles of void fraction, liquid droplet frequency and droplet velocity were acquired across the narrow test section dimension. Based upon these results, data for liquid droplet size were obtained and compared to previous experimental results from the literature. These data are useful for developing an improved understanding of practical two-phase refrigerant flows, and for assessment of advanced two-fluid computer codes.

Nomenclature

B	bias
C_w	coefficient defined by Equation 19
D_h	duct hydraulic diameter
d_d	droplet diameter
d_s	HFA probe sensor spacing
d_{sm}	Sauter mean droplet diameter
$E(\tau)$	cross-correlation factor
f_d	droplet frequency
G	mass flux
j	superficial velocity
$N\mu$	viscosity number
P	pressure
Q	volumetric flow rate
Re	Reynolds number
$S_{\bar{x}}$	precision index
t	duct thickness
t_{95}	student's t for 95% confidence
U	measurement uncertainty
V	HFA output voltage
V_d	droplet velocity
V_i	interfacial velocity
V_m	mixture velocity
V_T	threshold voltage for HFA probe signal analysis
W	duct width
We_m	modified Weber number
w	mass flow rate
X	streamwise (length) dimension
Y	transverse (width) dimension
Z	spacing (thickness) dimension

Greek Symbols

α	void fraction
$\Delta\rho$	density difference
μ	dynamic viscosity
ρ	density
σ	surface tension
τ_m	time associated with maximum cross-correlation factor

Subscripts

d	droplet
g	gas phase
l	liquid phase
2ϕ	two-phase (mixture)

Introduction

Application of two-fluid model computer codes for prediction of gas-liquid flows relies on the availability of an experimental database from which an understanding of fundamental physical phenomena can be developed. Such a database is also required to rigorously assess a code's predictive capability. Most of the experimental data in the open literature apply to air-water flows through circular geometries at atmospheric conditions. Detailed two-phase flow data for different fluids, in particular for low liquid-to-gas density ratios through noncircular geometries at elevated temperature and pressure conditions, are seriously lacking.

Annular two-phase flow usually occurs through a transition from the slug/churn-turbulent flow regime at high average void fractions. In such flows, the liquid phase is transported in both a film along the walls and as droplets entrained in the central gas core. The ratio of the liquid phase in the film to that in droplet form varies according to a number of parameters, including the fluid flow rates and the liquid-to-gas density ratio. The interface between the liquid film and the vapor core is characterized by disturbance (or roll) waves. These waves often have heights which are several times larger than the mean liquid film thickness, and can travel relative to the liquid film at significant velocities. At high gas velocities, the roll wave crests are sheared off, causing the entrainment of droplets into a highly turbulent vapor core. Droplets can also be formed by the disintegration of the liquid bridges in the churn-turbulent regime. The droplets thus formed are transferred and redeposited on the film.

Physically based models for annular two-phase flows account for the split of the liquid and vapor phases between continuous and dispersed fields. Hewitt and Hall-Taylor (1970) state that droplet size is important in determining the mass and heat transfer behavior of the system, and for determining the velocity of the droplets with respect to the gas phase. The inference is that the droplet size and velocity are usually not simultaneously measured. Indeed, measurements of both droplet size and droplet velocity profiles in annular flow have been reported in only a few publications (Hadded *et al.*, 1985; Tayali *et al.*, 1990; Azzopardi and Teixeira, 1994a;b). These previous measurements were made in air-water flows for a wide range flow rates using laser-based velocity and sizing techniques.

Ueda (1979) provided a droplet size correlation based on data obtained in air-water, various aqueous solutions, and low liquid-to-gas density ratio refrigerant flows. There have also been mechanistic models and correlations based on shearing of roll waves (e.g., Tatterson *et al.*, 1977; Kataoka *et al.*, 1983; Lopes and Dukler, 1985) which were developed primarily from air-water data at atmospheric conditions. These models tend to deviate from the experimental data for low liquid-to-gas density ratios. Kocamustafaogullari *et al.* (1994) developed a droplet size model accounting for the break-up of the droplets in addition to the shearing of the roll waves. Their model has not been tested against detailed local measurements of droplet size in heated systems, especially in geometries other than circular cross-sections. As pointed out by Lopes and Dukler, the location at which droplet sampling is made in the vapor core is critical for validating different models.

Few local measurements of droplet size, droplet velocity and void fraction are available for heated systems with low liquid-to-gas density ratios. In addition, the majority of open literature information involves circular pipes. The present study was undertaken to acquire local data in two-phase flows through a vertical duct geometry, at pressures significantly above atmospheric. This study expands upon earlier work (Trabold *et al.*, 1997) by concentrating attention on annular flow phenomena through the application of a variety of advanced instrumentation techniques. The working fluid for all the experiments was R-134a[1], one of the relatively new class of nonchlorinated refrigerant fluids which does not deplete the ozone layer. This fluid is widely used in heat exchangers, air conditioning and refrigeration systems, and is recommended as a replacement for R-113 and R-114. Aside from its practical importance, R-134a is also of scientific interest because of its very low liquid-to-vapor density ratio and low surface tension (7.3 and 0.0021 N/m, respectively, at 2.4 MPa).

The specific objectives of this study are to: 1) extend the annular flow database in refrigerant flows through a vertical duct at pressures much higher than atmospheric pressure; 2) provide

---

[1] 1,1,1,2-tetrafluoroethane

liquid droplet velocity and size measurements in the vapor core at liquid-to-gas density ratios comparable to steam-water at high pressure; and 3) understand the new data for void fraction, droplet frequency, velocity and size, and provide insight into the complex physical phenomena characteristic of annular two-phase flows.

Experimental Facility and Instrumentation

R-134a Loop and Test Section

Key components of the experimental R-134a loop are a chiller and pressurizer to maintain the liquid phase at the inlet of a circulating canned rotor pump, a large CO_2 heat exchanger, loop heaters, high/low range throttle valves, flow meters, and a vertical test section. Loop conditions are set by programmed logic controllers; acquired data include mass flow rate, temperature, pressure, heater power, and test section pressure drop. The loop design pressure ranges from 0.4 to 2.5 MPa, and temperature ranges from 0° to 80°C. The test section, illustrated schematically in Figure 1, has a hydraulic diameter of 4.85 mm. Optical access to the flow is provided by four pairs of fused silica windows. The center of the window width forms the transverse (Y) dimension of the flow passage. In the side of the test section between the pairs of windows are 2.5 cm diameter ports which permit access to the flow for various instruments. For these experiments, rakes of nine thermocouples were located in Ports #1 and 5. Three pressure taps were located within each window elevation, as well as at the top and bottom of the test section length.

A unique feature of the quartz windows is the presence of thin film heaters which enable testing with wall heat addition. The heater design consists of three transparent metallic oxide conductive films, vacuum deposited onto the inside surface, with an anti-reflective coating on the outside. Three silver epoxy buses carry the current around both ends of the windows, and connect with silver graphite brushes. Because the power to each of the three window heater strips is independently controlled, experiments can be performed with transverse and/or streamwise power profiles. The reported experiments were conducted under inlet-heated test conditions, so the window heater capability was not used.

An instrument scanning mechanism positions the gamma densitometer system (GDS) and laser Doppler velocimeter (LDV) instrumentation along three axes: the Z axis (horizontal scans along the test section spacing dimension), the Y axis (horizontal scans across the width of the test section) and the X axis (vertical, or streamwise position). To measure void distributions in either the thickness (Z) or the width (Y) directions, the gamma densitometer is rotated 90 degrees about the test section. Both gamma beam and laser tests have shown that the GDS and LDV positioning accuracy is approximately ±0.03 mm. A small offset in the measurement position (usually less than ±0.05 mm), introduced by thermal expansion of the test section, was corrected for as necessary.

The inlet to the test section is comprised of three independent flow zones which enable the introduction of different flow rates and/or fluid enthalpies. This feature permits the investigation of flows with nonuniform inlet boundary conditions. For all experiments documented in this paper, the inlet flow was introduced either entirely through the center zone, or evenly divided among the three zones. In the latter case, the fluid enthalpy was not varied across the test section inlet. The experimental results indicate that the manner in which the flow enters the test section has no discernible effect on measurements taken at downstream locations.

Gamma Densitometer System (GDS)

The gamma densitometer provides a direct measurement of the density of a two-phase mixture in the path of a gamma beam through the following relationship:

$$\rho_{2\phi} = \frac{\ln\left(\frac{I_o}{I}\right)}{\mu t} \tag{1}$$

where I_o and μt are calibration constants obtained from gamma count measurements at each desired measurement position, with an empty test section and a subcooled liquid-filled test section. I is the count rate measured for the two-phase test condition. The two-phase density is related to the void fraction and vapor and liquid densities through the following relationship:

$$\rho_{2\phi} = (1-\alpha)\rho_l + \alpha\rho_g \tag{2}$$

where α is the void fraction, ρ_l is the density of the liquid phase, and ρ_g is the density of the vapor phase. Solving for α yields:

$$\alpha = \frac{\rho_l - \rho_{2\phi}}{\rho_l - \rho_g} \tag{3}$$

The liquid and vapor phase densities are determined from a database for R-134a saturation properties at the measured test section exit temperature.

The GDS currently being used in the R-134a test facility features a 9 curie Cesium-137 gamma source and a NaI detector. The gamma beam width can be adjusted by rotating the source collimator with a remote selector switch. The gamma beam height is 1.9 cm for both source collimator positions. The wide beam, when directed through the edge of the test section (wide beam edge measurement), interrogates the entire cross-section of the fluid and yields a measurement of the cross-sectional average void fraction. A spacing (Z) dimension void fraction data scan is obtained using the narrow beam directed through the test section edge (narrow beam edge scan). The effective gamma beam width at the test section for a narrow beam edge scan is 0.43 mm. Typically, eight line-average void fraction measurements were made across the Z dimension of the test section. Another type of gamma densitometer measurement is the wide beam measurement through the thickness dimension of the test section. These measurements were performed at the centerline of the duct width (Y dimension), about 6.3 cm below the hot-film anemometer probe. The effective gamma beam width at the test section is 4.2 mm. This line-average void fraction measurement provided a means of assessing the accuracy of local void fraction measurements, through comparison to the integrated average of hot-film anemometer data. All three types of GDS data were obtained at a streamwise position of $X/D_h = 169$.

Hot-Film Anemometer (HFA)

The constant temperature hot-film anemometer technique was used previously for various two-phase flow measurements in R-114 and R-134a and is described in detail by Trabold *et al.* (1994; 1997). The single sensor HFA probes used in this previous work afforded measurements of both local void fraction and interfacial frequency profiles. For the present testing program, a dual-sensor probe was installed at $X/D_h = 182$ and the center of the Y dimension (Figure 1), through a hole in a quartz window (Figure 2). As illustrated in Figure 3, the HFA probe is comprised of two active sensing elements which are separated in the streamwise (X) dimension by a known distance. The probe used in the present tests had platinum film sensors with a 25 μm diameter and 254 μm active length, and a measured sensor separation distance of 1.44 ± 0.01 mm.

The use of two sensors permits acquisition of interfacial velocity measurements based on the cross-correlation between two output voltage signals:

$$E(\tau) = \lim_{T \to \infty} \frac{1}{T} \int_0^T V_1(t) V_2(t+\tau) dt \tag{4}$$

The peak in the $E(\tau)$ versus time plot corresponds to the most probable time required for a gas-liquid interface to travel between the HFA sensors (τ_m), from which the mean interfacial velocity may be calculated by

$$V_i = \frac{d_s}{\tau_m} \tag{5}$$

where d_s is the spacing between upstream and downstream HFA sensors.

A curved pin in the sensor probe is used to sense electrical contact with the opposite window heating element, and thereby defines the probe position near that wall. The offset between the contacting surface of the pin and the sensors is 0.08 ± 0.01 mm. Frequent contact between the probe and window caused the heater strip to eventually wear to the point that electrical continuity was no longer attainable. To provide a more rigorous contacting surface, a small 0.07 ± 0.01 mm thick silver epoxy spot was applied to the window. This design change eliminated the loss of electrical continuity, but also moved the measurement position nearest the wall to 0.15 mm. Because the flow field was expected to be symmetric about the center XY plane for these tests, HFA probe movement was limited to about $Z = 1.3$ mm.

The combined slope and level thresholding method of de Carvalho and Bergles (1992) was used to analyze the HFA output voltage signals for determination of local vapor volume fraction. A level threshold was set at the midpoint between the vapor and liquid parts of the output voltage signal, with slope thresholding additionally applied to account for the finite time for gas-liquid interfaces to pass the HFA sensor. Because this entire test sequence was devoted to investigation of annular flow phenomena, with cross sectional average void fractions generally exceeding 70%, it is appropriate to discuss the salient features of a typical HFA output voltage signal in this type of flow field. As illustrated in Figure 4, a characteristic continuous vapor and dispersed liquid signal is comprised of a fairly constant baseline voltage level with periodic positive pulses indicative of liquid droplets impacting the probe sensor. The rapid voltage rise observed upon impact of the front droplet interface is due to the cooling of the sensor element which decreases its resistance. An amplifier in the resistive bridge circuit increases the current through the sensor to maintain it at a constant temperature. The subsequent voltage decrease, which tends to be somewhat slower, is due to the heating of the droplet and penetration of the rear droplet interface. Previous researchers (e.g., Goldschmidt and Householder, 1969; Mahler and Mangus, 1984) observed for dispersed liquid experiments with water and oil that the droplets adhere to the HFA sensor element, heat up, and then evaporate. For SUVA droplets, it is considered unlikely that the same process occurs since the surface tension is lower and the motion of droplets above a certain critical size is not significantly impeded. The close agreement between droplet velocities obtained with the HFA probe via cross-correlation and the nonintrusive laser Doppler velocimetry technique, discussed below, tends to support this interpretation. Also, the droplet heating process is not as significant when the droplets are at or near the saturation temperature.

A typical output voltage sample histogram associated with a dispersed liquid/continuous vapor waveform is shown in Figure 4c. The large peak represents the baseline vapor phase voltage. Samples in voltage bins to the right of this peak correspond to discrete samples of the liquid droplet pulses. Depending on the magnitude of the dispersed liquid volume fraction, a smaller peak may also be visible at the high end of the output voltage range. If both vapor phase and liquid phase peaks are present, the analysis program selects the threshold voltage (V_T) at the midpoint between these peaks. If one of these peaks is absent, the analysis program first eliminates bins at high and low voltage extremes which contain fewer than 100 samples. This minimizes possible biasing due to the presence of a "tail" in the voltage histogram caused by spurious voltage spikes in the output signal. The threshold voltage is then taken as the median, i.e., midpoint between the highest and lowest voltage bins after the elimination process. This technique for determining the threshold voltage is somewhat arbitrary, since the actual residence time of liquid droplets at the HFA sensor is not known. However, as discussed below, the integrated averages of various HFA Z scan data profiles obtained were found to be in good agreement with line-average gamma densitometer measurements.

In addition to the local void fraction, the data analysis program also provided a measurement of local liquid droplet frequency by counting the number of positive pulses per known measurement time. This measurement is complicated due to the variable amplitude of the liquid droplet pulses, which results from different droplet sizes and eccentric droplet impaction on the HFA sensor. Although a few pulses extend above the threshold voltage level established for void fraction computation, some are of lower amplitude and extend a small amount beyond the random voltage fluctuations associated with the baseline voltage of the continuous vapor phase. If these droplets are not accounted for, a significant error results in the measured droplet frequency and in certain derived quantities such as droplet size. It is therefore necessary to establish a separate threshold voltage level for liquid droplet counting. The baseline vapor phase voltage is assumed to be well represented by a Gaussian distribution, as established from voltage data records obtained in pure liquid flow. Thus, the discrete voltage samples of the continuous vapor phase fall within the range V_{min} to $V_{min} + 2(V_{peak} - V_{min})$; the latter value is used as the threshold voltage for droplet frequency determination.

Laser Doppler Velocimeter (LDV)

Laser Doppler velocimetry is a well established instrument for velocity measurements in single-phase gas and liquid flows. This technique has also been used to simultaneously measure vapor and liquid velocities in bubbly flow (e.g., Vassallo *et al.*, 1993). In the present experiments, two focused laser beams were transmitted through a quartz window, to intersect inside the test section at $X/D_h = 169$ (Figures 1 and 2). This intersection point defines the measurement location within the droplet field. Measurement of droplet velocity requires that the two LDV beams penetrate the wall-bounded liquid film and intersect to form a well-defined measurement volume. Success depends on the thickness and steadiness of the film. At high void fractions and high flow rates, the liquid film is relatively thin, and LDV droplet measurements are possible across most of the test section Z dimension. As the void fraction or flow rate decreases, the film gets thicker and wavier, and the LDV measurements are more difficult to attain. At some moderate void fractions and flow rates, measurements of droplet velocity are only possible near the central plane of the test section. At low void fractions (less than 0.7), the irregularities in the film make it impossible to obtain any droplet measurements.

A backscatter fiber optic LDV probe was used to acquire the droplet velocity measurements. The probe was equipped with a short focal length lens (122 mm) to produce a measurement volume about 0.25 mm long. The probe was mounted on a traversing slide to enable motion in the test section thickness (Z) dimension. When droplet measurements were desired, the probe was moved forward toward the test section. The position at which Doppler signals first appeared was judged to be the near wall (i.e., the wall closest to the probe). Measurements were taken across the test section thickness dimension with a positioning uncertainty of about ±0.13 mm. The beam power at the probe exit was between 40 and 75 mW.

The Doppler signals were analyzed for velocity using a counter-timer signal processor. Input signals must first pass a voltage threshold; if a signal is greater than a minimum amplitude, it is processed for velocity. However, if the processor gain is set too high, noise may be misinterpreted as a valid signal. To ensure that the gain was not excessive during the experiments, a comparison check was employed to assess the repeatability of the time for each cycle within a given Doppler burst. Also, an additional data quality check was performed by occasionally blocking one of the LDV beams to confirm that the data rate fell to zero. If noise appeared in the velocity histograms (usually in the form of stray velocity samples separated from the main peak) it was removed using the data analysis software. These samples usually accounted for less than 10% of the total number of samples.

Typical data rates for the velocity measurements were between 2 and 20 Hz, depending on the measurement location inside the test section. Between 500 and 1000 velocity samples were obtained at each measurement location over a period of 2 to 5 minutes. LDV measurements were only taken across the near half of the test section Z dimension because of the difficulty in obtaining a reasonable data rate as the beams penetrated further into the test section.

Measurement Uncertainty

The measurement uncertainty for all test section instrumentation was calculated based on the root-sum-square uncertainty interval for 95% confidence:

$$U = \pm[B^2 + (t_{95}S_{\bar{x}})^2]^{1/2} \tag{6}$$

where B is the bias limit (systematic error) and $t_{95}S_{\bar{x}}$ is the precision limit (random error). The ranges of experimental parameters investigated, and the uncertainty associated with each, are summarized in Table 1.

Results and Discussion

The experimental results discussed in this section were obtained with a fixed nominal system pressure of 2.4 MPa. The two operating variables were mass flow rate (nominally 106, 266 and 532 kg/hr) and cross-sectional average void fraction (nominally 0.75, 0.85 and 0.94). After establishing the pressure and flow conditions, heaters immediately upstream of the test section were used to generate the desired void fraction, as measured with the gamma densitometer. The two-phase flow test condition was considered steady when this measurement stayed within its uncertainty band (±0.017 in void fraction) for a period of at least 30 minutes.

The majority of the results presented in this section correspond to data scans across the narrow (Z) test section dimension. The abscissa on most plots is the dimensionless distance from the wall, *Z/t*, where *t* is the thickness of the duct. Detailed local data were acquired with both the hot-film anemometer and laser Doppler velocimeter. The reported gamma densitometer data correspond to cross-sectional average measurements, and line-average measurements immediately below the HFA probe. Z dimension GDS scans were also obtained, but are not reported as the trends closely mirror those observed in the more detailed HFA profiles.

Local Void Fraction

As a means of assessing the validity of the local HFA void fraction measurements, simultaneous GDS line-average void fraction data were obtained for selected test runs. The gamma beam was directed through the narrow test section dimension immediately below the HFA probe, in the third window elevation ($X/D_h = 169$) at the test section centerline. The local HFA data were numerically integrated via the trapezoidal rule, and compared with the corresponding GDS data, as shown in Figure 5. The two data sets agreed within an average difference of 0.033 in void fraction, with a maximum difference of 0.066. This result provided confidence that the HFA probe was not significantly influencing the local flow field structure, and confirmed the thresholding method used to extract void fraction information from the raw output voltage signal.

The local void fraction results are presented in Figure 6. For each mass flow rate condition, data are plotted for the three nominal average void fractions investigated. The shape of the local void fraction variation is clearly a function of both mass flow rate (*w*) and cross-sectional average void fraction (α). For $\alpha = 0.94$, the local void fraction profiles are nearly flat over the duct cross-section, regardless of the magnitude of *w*. At $\alpha = 0.85$, void fraction is maximum at the duct centerline for $w = 106$ kg/hr (Figure 6a). As the flow rate is increased to 266 kg/hr (Figure 6b), a distinct change in the local void fraction variation is observed. The maximum in the profile exists around $Z/t = 0.15$, and the minimum void fraction (i.e., largest liquid volume fraction) is measured at the duct centerline. At w = 532 kg/hr (Figure 6c), the peak void fraction is measured at the near-wall measurement position, with a local minimum again measured at the center of the flow field.

For $\alpha = 0.75$, the void fraction profile is center peaked at $w = 106$ kg/hr and 266 kg//hr (Figures 6a and 6b), but again displays a near-wall maximum for the highest mass flow ($w = 532$ kg/hr; Figure 6c). The significant "inversions" in these void fraction profiles were also captured by the simultaneous gamma densitometer data scans, but are not reported here. This unexpected behavior results from the apparent thinning of the liquid film with increasing mass flow, as observed on the high-speed video record. With a very thin liquid film and small amplitude interfacial wave structure, the local void fraction depends solely on the transport of the dispersed liquid droplet field. It is pertinent to note that for $\alpha = 0.75$, the measured centerline dispersed liquid droplet velocity changes from about 1 to 4 m/s with a mass flow rate increase from 106 to 532 kg/hr. The apparent inversion in the void fraction profile with increasing mass flow rate is related to this increase in velocity and measured droplet frequency.

The void fraction data for $\alpha = 0.75$ and 0.85 at $w = 532$ kg/hr are interesting because the profiles indicate the presence of a thin liquid film, with a significant fraction of the liquid phase transported in the dispersed droplet field. The entrainment fraction (E), defined as the ratio of liquid mass flow rate in the entrained (droplet) phase to the total liquid mass flow rate, has been previously investigated. Recently, Lopez de Bertodano *et al.* (1995) proposed a simple entrainment fraction correlation:

$$E = \frac{1}{1 + \frac{3845}{We_c}} \tag{7}$$

where

$$We_c = \text{gas core Weber number} = \frac{\rho_{gc} j_g^2 D}{\sigma} \tag{8}$$

with ρ_{gc} being the mixture density in the gas core. Equation 7 was demonstrated to reasonably represent both low pressure air-water data (Cousins and Hewitt, 1968), as well as high pressure steam-water data (Keeys *et al.*, 1970; Wurtz, 1978). Using this expression, E for the three test runs at w = 532 kg/hr (Figure 6c) was calculated to be 0.54, 0.58 and 0.73 for $\alpha = 0.75$, 0.85 and 0.94, respectively. These values are significant because most of the low pressure air-water data for entrainment fraction fall in the $0.05 < E < 0.3$ range, while the high pressure data extend over the $0.4 < E < 0.9$ range. The entrainment fractions associated with R-134a at high mass flow rate appear to be more in line with those measured for high pressure systems. This is likely due to the fact that gas phase density and surface tension for R-134a (130.5 kg/m^3 and 0.0021 N/m, respectively, at 2.4 MPa) are much different than for air-water flows; both properties act to increase the value of the gas core Weber number. It is possible that if detailed local void fraction measurements were available for steam-water flows in which the entrainment fraction exceeds 0.5, similar void fraction inversions would be observed.

Droplet Frequency

A separate threshold voltage (V_T) was used for measurement of liquid droplet frequency, based on an assumed Gaussian distribution of continuous vapor phase voltage samples. Also, during the course of this test, it was discovered that a faster digitizing rate of the HFA output voltage signal was required to accurately measure the droplet frequency, f_d. Although most previous testing had been conducted using a 10 kHz rate, 50 kHz was required in the annular flow experiments to resolve droplets that, for $w = 532$ kg/hr, had velocities in excess of 6 m/s. Therefore, f_d data are reported only for experimental runs conducted with a 50 kHz digitizing rate.

The droplet frequency measurement is complicated by the variable amplitude of the "pulses" in the output voltage signal (Figure 4a). Large droplets which strike the HFA sensor directly produce large amplitude pulses, while small droplets (some of which have a size close to that of the 25 μm diameter sensor) or "glancing" interactions of large droplets produce smaller voltage signals. These smaller signals are more difficult to resolve because of the random fluctuations in the baseline voltage associated with the continuous vapor phase, and due to the inherent noise of the data acquisition system. Goldschmidt (1965) used a hot-wire probe to measure liquid particle concentration in a two-phase jet. He found that under some conditions the "impaction coefficient" (defined as the ratio of particles counted per time to the particles flowing per time through an area equal to that of the wire facing the stream) was less than unity. Later, Goldschmidt and Eskinazi (1966) determined that the impaction coefficient is independent of both local velocity and particle size distribution. In the present experiments, it is reasonable to expect that not all liquid droplets striking the HFA sensor produce countable pulses. Additionally, large droplets are less likely to produce such signals than are small droplets.

The droplet frequency data are presented in Figure 7 for mass flow rates of 106, 266 and 532 kg/hr, and nominal cross-sectional average void fractions of 0.75, 0.85 and 0.94. Measured frequencies may be somewhat less than the actual droplet concentration in the flow, and calculation of derived quantities (i.e., droplet diameter) may involve some bias toward larger droplets. The influence of this bias is discussed further below. For $w = 106$ kg/hr, the droplet frequencies in Figure 7a are at least an order of magnitude lower than for the two higher mass flow rates, and nearly constant across the duct spacing dimension. A slight increase in f_d is consistently observed upon moving from the near-wall region toward the duct centerline. Additionally, for $w = 106$ kg/hr, it appears that the data for all three average void fractions could be well represented by similar functions. For $w = 266$ kg/hr, the droplet frequency profiles for $\alpha = 0.85$ and 0.94 (Figure 7b) are nonlinear with the frequency doubling for the higher void fraction. For $\alpha = 0.75$, only a 10 kHz HFA digitizing rate was used. Therefore, droplet frequency data were not obtained for this condition.

For the highest mass flow rate test condition (532 kg/hr), the situation becomes more complex because the shapes of the droplet frequency profiles are more dependent on the magnitude of the average void fraction. For $\alpha = 0.85$ (Figure 7c), the f_d trend is similar to that observed for the lower flows. Upon increasing the average void fraction to 0.94, a steady increase is seen in the droplet frequency from the wall to the duct centerline, with no apparent flattening of the profile. Over most of the duct cross-section, the measured droplet frequency is less than that for $\alpha = 0.85$, with approximately a 15% increase in frequency at the duct centerline for the higher void fraction conditions. For $\alpha = 0.75$, a maximum in f_d is observed at about $Z/t = 0.15$, with a monotonic decrease measured upon moving toward the duct centerline. This result seems contradictory to the void fraction "inversion" observed for this case (Figure 6c), because of the supposition that a lower droplet frequency implies a greater vapor volume fraction. However, as discussed later, the decrease in both void fraction and droplet frequency may be associated with a different droplet generation mechanism which produces relatively large diameter droplets.

Droplet Velocity

Droplet velocity profiles measured across half the test section thickness dimension, using the dual-sensor HFA and LDV techniques, are provided in Figure 8 for all mass flow rates tested. For $\alpha = 0.85$, only LDV velocity data were obtained. For all experiments conducted with $\alpha = 0.75$ and 0.94, there is good agreement between the two sets of data, especially near the duct centerline ($Z/t = 0.5$). In the near-wall region ($Z/t < 0.2$), the data sets differ somewhat, with the HFA data being the higher velocity in all cases except for the two lowest mass flow rates at $\alpha = 0.75$ (Figure 8a). These variations may be attributable to inherent differences in the two measurement techniques. The effective size of the measurement volume in the Z dimension (approximately 0.25 mm for LDV and 0.03 mm for HFA) can influence the measurement of mean velocity, especially in a region of large velocity gradient. Additionally, because the LDV measurement is spatially averaged over 0.25 mm, about one-tenth of the duct spacing dimension, it is possible that in the near-wall region both liquid droplets and slower interfacial waves are measured, thereby causing a negative bias in the mean velocity. For the experiments with $\alpha = 0.94$, where the wall-bounded liquid film is thinner, the LDV and HFA data are in closer agreement.

From the outset, it was assumed that the annular flows investigated are two-dimensional, and the measurements made in the duct center are representative of the droplet core measurements. To confirm the two-dimensionality, LDV measurements were taken at $Z/t = 0.5$ across the width (Y dimension) for selected conditions (Figure 9). These figures suggest that the droplet velocity profiles are essentially flat across the width, except close to the edges where a thicker film and possibly bigger droplet size lower the droplet velocity. Therefore, the measurements made with the HFA at $Y/W = 0.5$ are valid and representative of core annular flow measurements, and can be used for comparison and validation of developed models. Also, it is also noteworthy that both Y and Z dimension velocity profiles were repeatable to within a few percent.

Droplet Size

In previous work involving bubbly R-114 flows (Trabold *et al.*, 1994), an expression was used to calculate the bubble diameter, based on local void fraction, frequency and velocity measurements. A similar expression can be derived for the dispersed liquid droplet diameter, d_d, which utilizes the HFA probe measurements. Assuming a cylindrical control volume is centered around the hot-film anemometer probe and the probe is exposed to only the continuous vapor (cv) and dispersed liquid (dl) fields, the local liquid volumetric flow rate through this control volume may be written as

$$\dot{Q}_l = Q_d f_d \tag{9}$$

where Q_d and f_d are, respectively, the average liquid droplet volume and droplet frequency. Alternatively,

$$\dot{Q}_l = V_d A_d \tag{10}$$

where V_d and A_d are the time-average droplet velocity and the average droplet cross-sectional area. For a predominantly one-dimensional flow, the ratio of liquid volume to total volume becomes an area ratio and hence,

$$\alpha_{dl} = \frac{A_d}{A_T} \tag{11}$$

where α_{dl} is the volume fraction of the dispersed liquid field and A_T is the total cross-sectional area of the cylindrical control volume. Substituting Equation 11 and equating Equations 9 and 10 results in

$$Q_d f_d = V_d \alpha_{dl} A_T \tag{12}$$

Simplifying by assuming that all liquid droplets are spherical, an expression for d_d becomes

$$d_d = 1.5\frac{V_d(1-\alpha)}{f_d} \tag{13}$$

where α and f_d are measured by the upstream sensor of the HFA probe (Figures 6 and 7, respectively), and the time-average liquid droplet velocity V_d is obtained from the LDV and from the cross-correlation between the two HFA output voltage signals (Figure 8).

Droplet size calculations are not reported for spacing positions where the presence of the wall and liquid film may have influenced the random motion of the droplet field, thereby invalidating one of the assumptions invoked in deriving Equation 13. As illustrated by Kalkach-Navarro *et al.* (1992) for bubble size measurements, the probe position must be greater than one bubble diameter from the wall. Hence, to satisfy this criterion for all of the present test conditions, droplet diameter data are presented only for $Z/t > 0.2$.

The dispersed liquid droplet diameter data for three mass flow rates at $\alpha = 0.75$, 0.85 and 0.94, calculated via Equation 13, are illustrated in Figure 10. No droplet size data are available for $\alpha = 0.75$ at 266 kg/hr because no droplet frequency measurements were acquired. The most obvious trend is that the droplet diameter generally decreases with increasing average void fraction. Also, because d_d varies as $1 - \alpha$, the shape of the diameter profiles tend to follow a trend which is the inverse of that observed for the local void fraction, as in most cases the gradients in measured droplet frequency and velocity are small for $Z/t > 0.2$. For the cases at $w = 106$ kg/hr with $\alpha = 0.75$ and 0.85 where center-peaked void fraction profiles were observed, the droplets appear to be larger in the vicinity of the co-flowing liquid film and smaller near the duct centerline (Figure 10a). The droplets are likely generated near the interface between liquid film and continuous vapor, due to the shearing of the roll waves.As discussed by Kocamustafaogullari *et al.* (1994), droplet size is controlled by the interaction between the droplet and the surrounding turbulent gas stream. Hence, newly entrained droplets measured near the liquid film are larger, while droplets at the duct centerline are subjected to turbulent break-up and would, on average, be smaller. Conversely, for test conditions where wall-peaked void profiles were measured, the corresponding mean droplet diameter is significantly larger near $Z/t = 0.5$ (Figures 10b, 10c). Several researchers (e.g., Tayali *et al.*, 1990; Azzopardi and Teixeira, 1994a) have reported that droplet sizes measured in circular pipes increase upon moving from the pipe wall to the centerline. For the present experiments, this trend may be the result of physical processes which are characteristic of the duct cross-section. For void fractions of 0.75 and 0.85 at mass flow rates of 266 and 532 kg/hr, the flow may be in the late stages of transition to annular flow, with liquid bridges extending across the narrow test section dimension. As these bridges are shattered by the high velocity vapor, relatively large droplets are produced away from the liquid films on the test section walls. Because the liquid film is thinner in the middle of the duct, it is also possible that droplets emanate from the edges where the film is considerably thicker. Consequently, larger droplets emerge from the roll waves at the edges than those arising from the thinner films on the wide walls of the test section. At $\alpha = 0.94$ for all three flow rates, the annular flow is fully developed and the droplet size is fairly constant across the duct.

In Figure 11a, the data are replotted to illustrate the relationship between droplet diameter and velocity. Droplet velocities normalized in terms of two-phase mixture velocity are also plotted in Figure 11b as a function of dimensionless droplet diameter. Mixture velocity is given by:

$$V_m = \frac{G}{\rho_{2\phi}} \quad \text{where} \quad \rho_{2\phi} = \rho_g \alpha + \rho_l (1-\alpha), \tag{14}$$

In general, for high void fractions, the droplet velocity is approximately the same as the mixture velocity. At lower void fractions, particularly for low flows, the droplet velocity tends to be higher than the mixture velocity. This is because the mixture velocity calculation includes a larger percentage of the film mass flux, and the film travels at a significantly lower velocity than the gas core. Also, HFA measures the droplet velocity only in the middle of the flat section, and therefore tends to be higher than the mixture velocity. The droplet velocities measured closer to the edges at this void fraction are indeed smaller than the peak velocity (Figure 9), and also the mixture velocity. It is reasonable to conjecture that at $\alpha = 0.75$ for all flow rates, the flow is somewhat locally annular since it is still undergoing late stages of transition. Here, a thinner vapor core is present in the middle of the test section and a thicker film, especially at the edges, breaks up into liquid bridges.

Several correlations for mean droplet size in annular flows are available in the literature. For example, Tatterson *et al.* (1977) proposed a correlation based on continuous gas phase kinetic energy and Reynolds number:

$$\frac{d_d}{D_h} \sim \left(\frac{\sigma}{\rho_g V_g^2 D_h}\right)^{0.5} \left(\frac{D_h \rho_g \langle j_g \rangle}{\mu_g}\right)^n \tag{15}$$

Ueda (1981) found that this relation inadequately represented data obtained in R-113 flows through a 10 mm diameter pipe, primarily due to the relatively large vapor phase density. By introducing the vapor-to-liquid density ratio, an improved correlation was derived to describe data for a variety of fluids, including R-113, water and aqueous glycerol solutions:

$$\frac{d_m}{D_h} = 5.8 \times 10^{-3} \left[\frac{\sigma}{\mu_g \langle j_g \rangle}\left(\frac{\rho_g}{\rho_l}\right)^{1.25}\right]^{0.34} \tag{16}$$

In this case, d_m is the volume weighted droplet diameter, represented by

$$d_m = \left[\frac{\sum d^3}{\sum d}\right]^{\frac{1}{2}} \tag{17}$$

More recently, Kocamustafaogullari *et al.* (1994) developed an expression for the Sauter mean droplet diameter, by considering the maximum stable droplet size in the turbulent vapor core:

$$\frac{d_{sm}}{D_h} = 0.65 C_w^{-\frac{4}{15}} We_m^{-\frac{3}{5}} \left(\frac{Re_g^4}{Re_l}\right)^{\frac{1}{15}} \left[\left(\frac{\rho_g}{\rho_l}\right)\left(\frac{\mu_g}{\mu_l}\right)\right]^{\frac{4}{15}} \left(\frac{\Delta\rho}{\rho_l}\right)^{-\frac{3}{5}} = 0.65K \tag{18}$$

where:

$$C_w = \frac{1}{35.34 N\mu^{0.8}} \quad \text{for } N\mu \leq \frac{1}{15} \tag{19}$$

$$N\mu = \text{viscosity number} = \frac{\mu_f}{\left[\rho_f \sigma \left(\frac{\sigma}{g\Delta\rho}\right)^{\frac{1}{2}}\right]^{\frac{1}{2}}} \tag{20}$$

$$We_m = \text{modified Weber number} = \frac{\rho_g D_h \langle j_g \rangle^2}{\sigma} \quad (21)$$

$$Re_f = \text{liquid Reynolds number} = \frac{\rho_f D_h \langle j_f \rangle}{\mu_f}, \text{ and} \quad (22)$$

$$Re_g = \text{gas Reynolds number} = \frac{\rho_g D_h \langle j_g \rangle}{\mu_g} . \quad (23)$$

It is instructive to compare the present R-134a data with other open literature results as well as the relation of Kocamustafaogullari *et al.* (Equation 18), because the latter has been demonstrated to reasonably predict droplet diameters in a variety of flows having wide ranges of physical properties. In order to apply Equation 18 for fluids having small density ratios, such as refrigerant fluids, the term $(\Delta\rho/\rho_f)^{-3/5}$ has been added to the right-hand side. This dimensionless parameter was omitted by Kocamustafaogullari *et al.* from the development of Equation 18, based on the assumption that $\rho_f >> \rho_g$. However, for R-134a at 2.4 MPa, the vapor and liquid densities are 130 and 953.1 kg/m^3, respectively, so it is appropriate to include $(\Delta\rho/\rho_f)^{-3/5}$ in the droplet diameter expression. This term increases by 9.2% the calculated mean diameters for R-134a, but has no significant effect on these calculations for air-water and other similar systems.

As discussed above, the present droplet size data are calculated from measurements of void fraction, velocity and droplet frequency. The void fraction and velocity results were confirmed by simultaneous measurements with a gamma densitometer and laser Doppler velocimeter, respectively. However, no such concomitant measurement exists for droplet frequency. If all droplets striking the HFA sensor were counted, the droplet diameter from Equation 13 would be an arithmetic mean. Based on the work of Goldschmidt (1965) and others, it is reasonable to expect that some droplet impactions do not result in countable voltage pulses. Hence, the calculated mean droplet size is biased toward larger droplets. Because the actual droplet size distribution is not known, it is reasonable to compare this diameter to measurements and correlations provided in terms of the Sauter mean diameter.

A comparison among the average R-134a droplet diameter measurements, other open literature measurements and the relation proposed by Kocamustafaogullari *et al.* is illustrated in Figure 12. The parameter K (Equation 18) was calculated using R-134a physical properties at a saturation pressure of 2.4 MPa. The present data correspond to the integrated average of measurements obtained at spacing measurement positions $Z/t > 0.020$; data obtained at near-wall positions were omitted due to the potential for bias associated with the presence of the wall-bounded liquid film or nonrandom droplet motion. The calculated mean droplet size for the test run conducted at $w = 532$ kg/hr with $\alpha = 0.75$ is not included in Figure 12. As mentioned previously, for this condition the significantly higher droplet size near the duct centerline is most likely the result of a different mechanism for droplet formation. Therefore, it is not reasonable to compare this data point with results for fully developed annular flows.

The data plotted in Figure 12, from both the present R-134a experiments and previous tests, show an appreciable amount of scatter about the line representing Equation 18, but this relation reasonably describes the overall trend in the data. This is significant because of the wide variety of fluid physical properties, gas and liquid flow rates and duct geometries investigated, and the various measurement techniques employed (Table 2). Perhaps the most encouraging aspect of this data comparison is that the liquid-to-gas density ratio varied from 7.3 for R-134a to 3700 in the helium-water experiments of Jepson *et al.* (1989). These results suggest that the relations developed by Kocamustafaogullari *et al.* (1994) can be used to estimate the mean droplet size in various practical two-phase flow systems, in particular pressurized steam-water flows which have physical properties similar to those of R-134a.

Conclusions

Local data for void fraction, droplet frequency and droplet velocity were obtained for annular flows of R-134a in a vertical duct. The void fraction and velocity measurements acquired using the dual-sensor hot-film anemometer method were confirmed through simultaneous measurements with nonintrusive gamma densitometer and laser Doppler velocimeter systems. It was observed that the shapes of the void fraction and frequency distributions are strongly influenced by mass flow rate. Notably, at relatively high flows, the measured void fraction was highest near the wall, due to the thinning of the liquid film and significant droplet entrainment. Based on data available in the literature, at relatively high mass flows R-134a appears to have entrainment fractions which fall in the range measured for pressurized steam-water systems. The local diameter of liquid droplets dispersed in the vapor core was calculated from measurements of void fraction, frequency and velocity. Despite the unusually low liquid-to-vapor density ratio and low liquid surface tension, the relationship derived by Kocamustafaogullari *et al.* (1994) is reasonably accurate for prediction of the present mean droplet diameter results. The local measurements reported in this paper are useful for modeling high pressure two-phase flows, and for assessment of two-fluid model computer codes.

Acknowledgments

The authors acknowledge the valuable contributions of Messrs. D.M. Considine, W.O. Morris, L. Jandzio, C.W. Zarnofsky and E. Hurd in the operation of the test facility, and advanced instrumentation data acquisition and analysis. Dr. G.J. Kirouac is acknowledged for his overall direction of the R-134a experimental program.

References

Azzopardi, B.J. and Teixeira, J.C.F., "Detailed Measurements of Vertical Annular Two-Phase Flow - Part I: Drop Velocities and Sizes," *ASME J. Fluids Eng.*, Vol 116, pp. 792-795 (1994a).

Azzopardi, B.J. and Teixeira, J.C.F., "Detailed Measurements of Vertical Annular Two-Phase Flow - Part II: Gas Core Turbulence," *ASME J. Fluids Eng.*, Vol 116, pp. 796-800 (1994b).

Cousins, L.B. and Hewitt, G.F., "Liquid Phase Mass Transfer in Annular Two-Phase Flow: Droplet Deposition and Liquid Entrainment," UKAEA Report AERE-R5657 (1968).

de Carvalho, R. and Bergles, A.E., "The Pool Nucleate Boiling and Critical Heat Flux of Vertically Oriented, Small Heaters Boiling on One Side," Rensselaer Polytechnic Institute, Heat Transfer Laboratory Report HTL-12, August 1992.

Fore, L.B. and Dukler, A.E., "The Distribution of Drop Size and Velocity in Gas-Liquid Annular Flow," *Int. J. Multiphase Flow*, Vol. 21, pp. 137-149 (1995).

Goldschmidt, V.W., "Measurement of Aerosol Concentrations with a Hot Wire Anemometer," *J. Colloid Sci.*, Vol. 20, pp. 617-634 (1965).

Goldschmidt, V.W. and Eskinazi, S., "Two-Phase Turbulent Flow in a Plane Jet," *ASME J. Appl. Mech.*, Vol. 33, pp. 735-747 (1966).

Goldschmidt, V.W. and Householder, M.K., "The Hot Wire Anemometer as an Aerosol Droplet Size Sampler," *Atmospheric Environment*, Vol. 3, pp. 643-651 (1969).

Hadded, O., Bates, C.J. and Yeoman, M.L., "Simultaneous Two-Phase Flow Measurement of Droplet Size and Velocity in a 32 mm Diameter Pipe," *International Symposium on Laser Anemometry*, FED-Vol. 33, pp.103-109, ASME (1985).

Hewitt, G.F. and Hall-Taylor, N.S., *Annular Two-Phase Flow*, Pergamon Press (1970).

Jepson, D.M., Azzopardi, B.J. and Whalley, P.B., "The Effect of Gas Properties on Drops in Annular Flow," *Int. J. Multiphase Flow*, Vol. 15, pp. 327-339 (1989).

Kalkach-Navarro, S., Lahey, R.T., Jr., and Drew, D.A., "Interfacial Density, Mean Radius and Number Density Measurements in Bubbly Two-Phase Flow," National Heat Transfer Conference, ANS Proceedings, HTC-Vol. 6, pp. 293-300 (1992).

Kataoka, I., Ishii, M. and Mishima, K., "Generation and Size Distribution of Droplet in Annular Two-Phase Flow," *ASME J. Fluids Eng.*, Vol. 105, pp. 230-238 (1983).

Keeys, R.K.F., Ralph, J.C. and Roberts, D., "Liquid Entrainment in Adiabatic Steam-Water Flow at 500 and 1000 p.s.i.a.," AERE-R629 (1970).

Kocamustafaogullari, G., Smits, S.R. and Razi, J., "Maximum and Mean Droplet Sizes in Annular Two-Phase Flow," *Int. J. Heat Mass Transfer*, Vol. 37, pp. 955-965 (1994).

Lopes, J.C.B. and Dukler, A.E., "Droplet Entrainment in Vertical Annular Flow and its Contribution to Momentum Transfer," *AIChE J.*, Vol. 32, pp. 1500 (1986).

Lopez de Bertodano, M.A., Jan, C.-S. and Beus, S.G., "Droplet Entrainment Correlation for High Pressure Annular Two-Phase Flow," *ANS Proceedings, National Heat Transfer Conference*, Vol. 8, pp. 3-10 (1995).

Mahler, D.S. and Magnus, D.E., "Hot-Wire Technique for Droplet Measurements," *Liquid Particle Size Measurements*, ASTM STP 848, J.M. Tishkoff *et al.* (eds.), American Society for Testing and Materials, pp. 153-165 (1984).

Tatterson, D.C., Dallman, J.C. and Hanratty, T.J., "Drop Sizes in Annular Gas-Liquid Flows." *AIChE J.*, Vol. 23, pp. 68-76 (1977).

Tayali, N.E., Bates, C.J. and Yeoman, M.L., "Drop Size and Velocity Measurements in Vertical Developing Annular Two-Phase Flow," *Laser Anemometry - Proceedings of the 3rd International Conference*, J.T. Turner (Ed.), pp. 431-440, Springer-Verlag (1990).

Trabold, T.A., Moore, W.E., Morris, W.O., Symolon, P.D., Vassallo, P.F. and Kirouac, G.J., "Two Phase Flow of Freon in a Vertical Rectangular Duct. Part II: Local Void Fraction and Bubble Size Measurements," *Experimental and Computational Aspects of Validation of Multiphase Flow CFD Codes*, I. Celik *et al.* (Ed.), FED-Vol. 180, pp. 67-76, ASME (1994).

Trabold, T.A., Moore, W.E. and Morris, W.O., "Hot-Film Anemometer Measurements in Adiabatic Two-Phase Refrigerant Flow through a Vertical Duct," ASME Fluids Engineering Division Summer Meeting, Vancouver, B.C., Paper FEDSM97-3518 (1997).

Ueda, T., "Entrainment Rate and Size of Entrained Droplets in Annular Two-Phase Flow," *Bull. JSME*, Vol. 22, pp.1258-1265 (1979).

Vassallo, P.F., Trabold, T.A, Moore, W.E. and Kirouac, G.J., "Measurement of Velocities in Gas-Liquid Two-Phase Flow Using Laser Doppler Velocimetry," *Experiments in Fluids*, Vol. 15, pp. 227-230 (1993).

Wicks, M. and Dukler, A.E., "In Situ Measurements of Drop Size Distribution in Two-Phase Flow - A New Method for Electrically Conducting Liquids," *Proc. of the 3rd Int. Heat Transfer Conf.*, Vol. 5, pp. 39-49 (1966).

Wurtz, J., "An Experimental and Theoretical Investigation of Annular Steam-Water Flow in Tubes and Annuli at 30 to 90 bar," RISO Report No. 371 (1978).

Table 1 - Experimental Parameters and Measurement Uncertainties

Measurement	Instrument	Parameter Range	Uncertainty Sources Considered	Uncertainty Band
test section absolute pressure	pressure transducer	2.4 MPa	• transducer accuracy • biases: transducer stability, static pressure effect, ambient temperature, data acquisition system accuracy	±0.02 MPa
mass flow rate	venturi with pressure transducer	106 to 532 kg/hr	• same as above • venturi calibration	±3.2 kg/hr
cross-sectional average void fraction	gamma densitometer	0.75 to 0.94	• gamma count repeatability • liquid and vapor density variations during calibration and measurement	±0.017
line-average void fraction (through Z dimension)	gamma densitometer	0.64 to 0.93	• same as cross-sectional average void fraction	±0.108
local void fraction	hot-film anemometer	0.40 to 0.99	• repeatability based on pooled standard deviation • biases: threshold voltage, small droplets, position, sampling time	±0.025
local droplet frequency	hot-film anemometer	100 to 4600 Hz	• same as void fraction • also, droplet impaction bias	-79 to +90 Hz at w = 106 kg/hr -321 to +652 Hz at w = 532 kg/hr
local droplet velocity	hot-film anemometer	0.44 to 6.14 m/s	• repeatability • biases: velocity sampling, droplet size, cross-correlation, sensor spacing, position	-7.5% to +7.0% (near wall) -7.0% to +6.4% (far wall)
local droplet velocity	laser Doppler velocimeter	0.59 to 6.42 m/s	• precision based on rms of mean velocity • biases: velocity sampling, random noise, position	-16.2% to +15.2% (near wall) -8.4% to +6.2% (far wall)

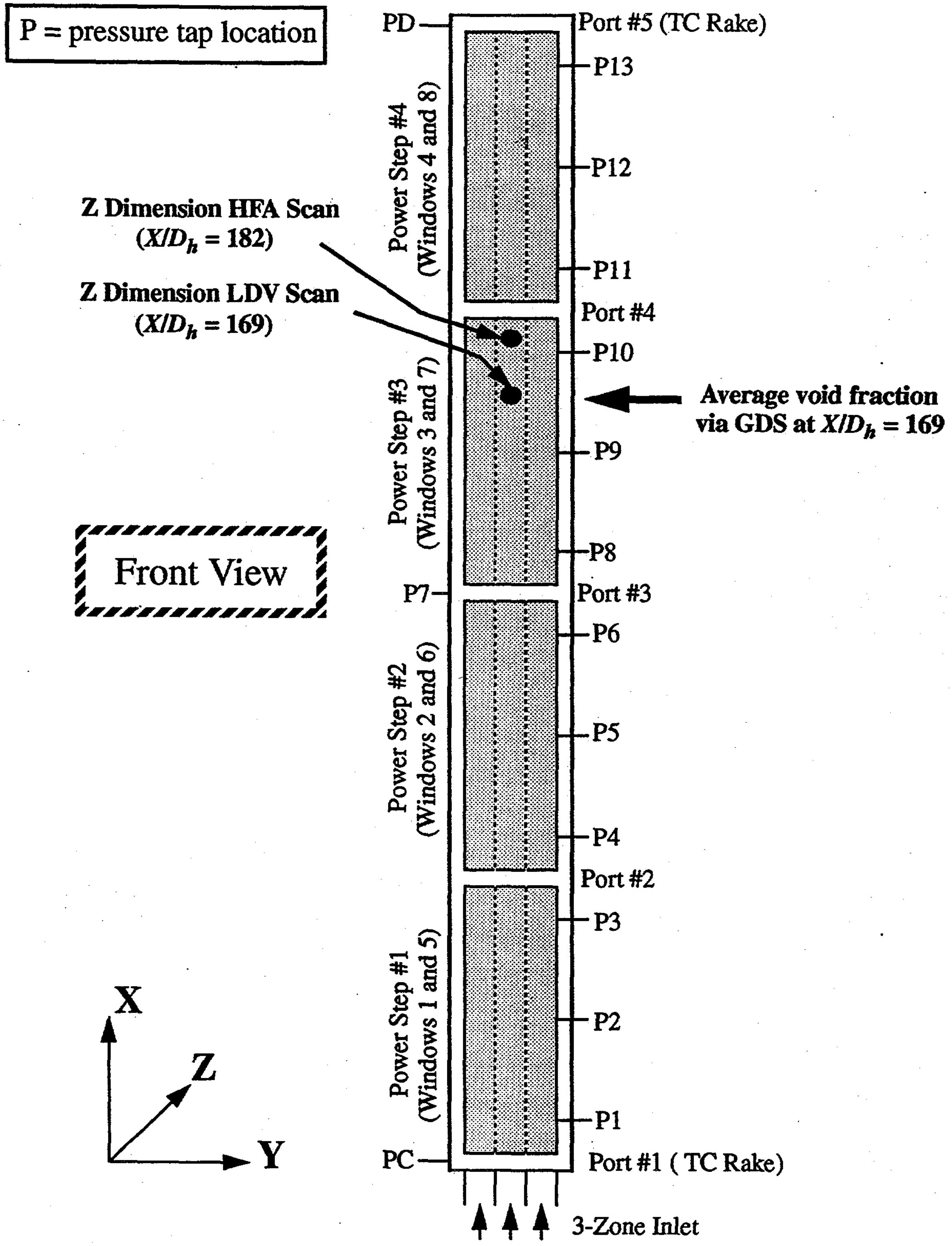

Figure 1 - Test Section and Measurement Locations

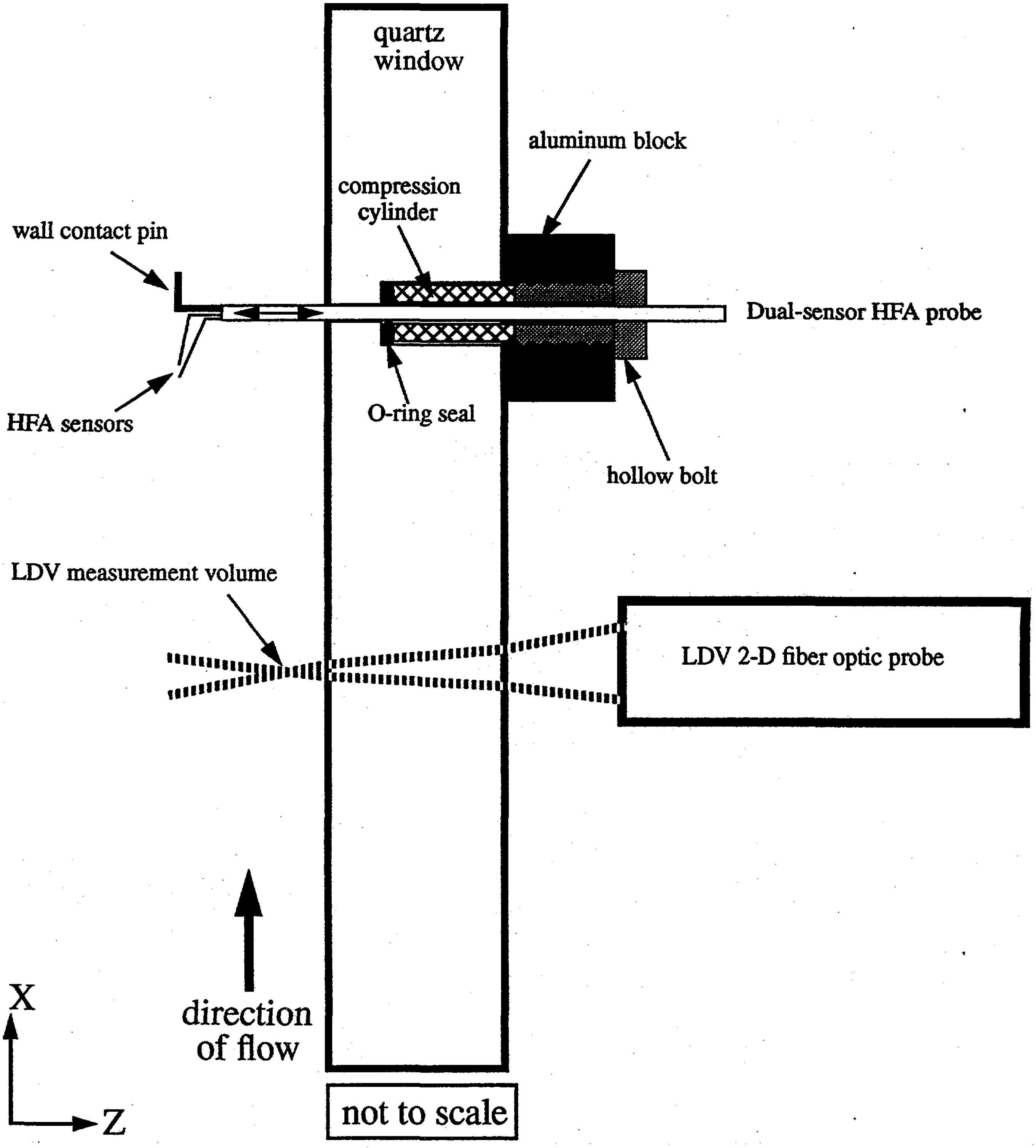

Figure 2 - Installation of HFA and LDV Instrumentation

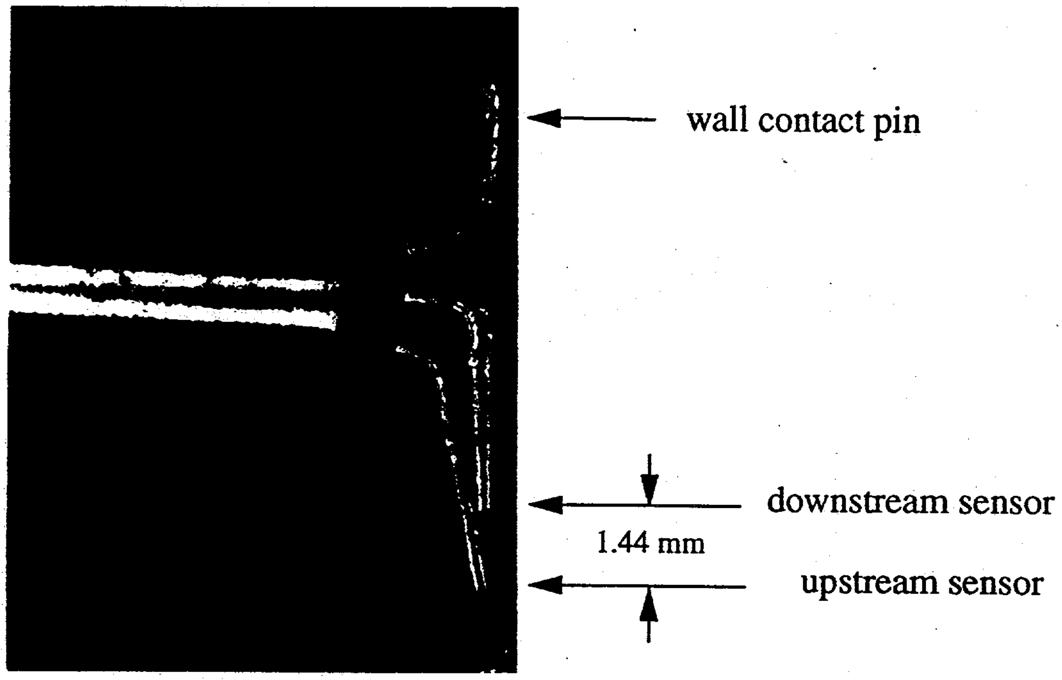

Figure 3 - Photograph of Dual-Sensor HFA Probe (7.5X magnification)

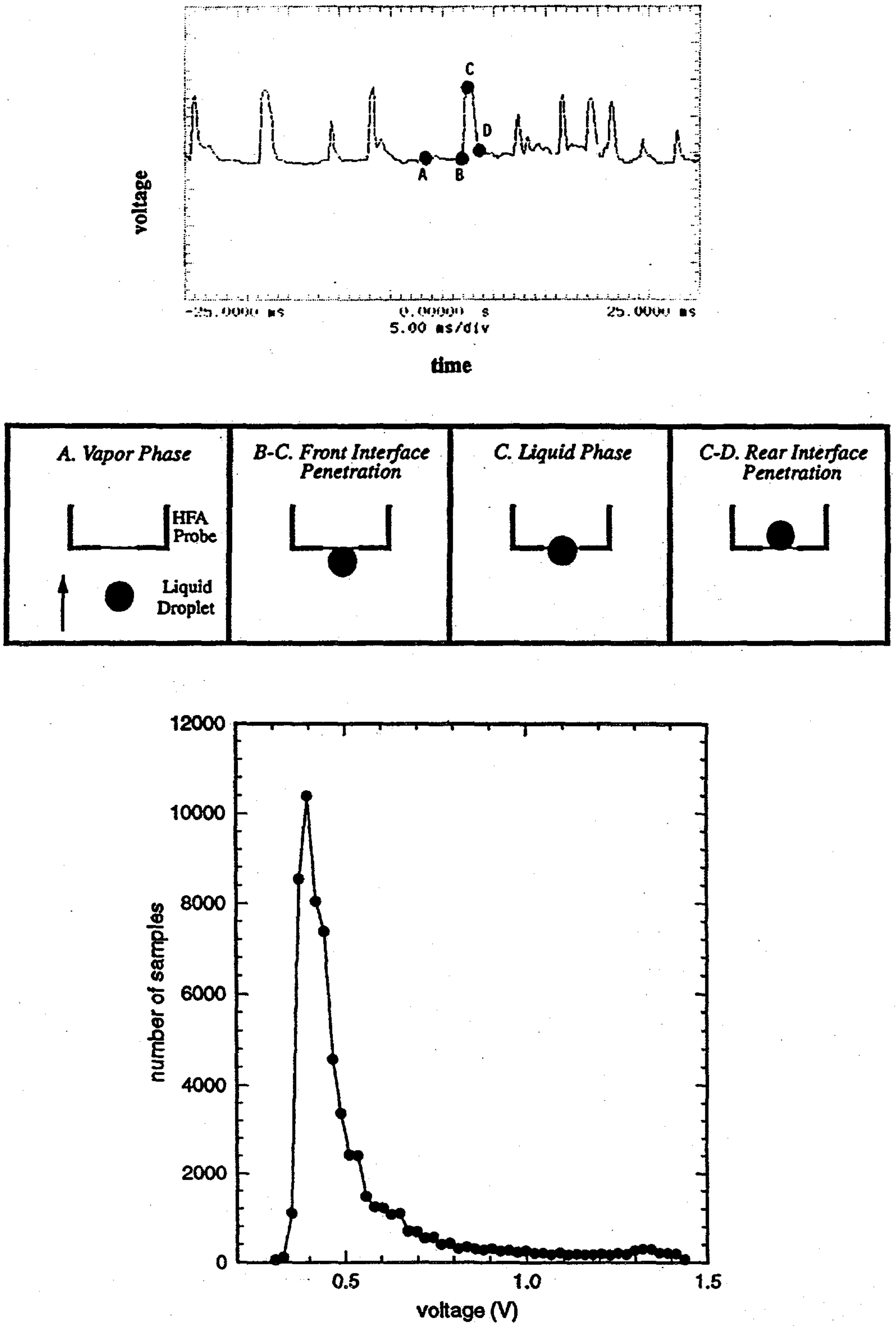

Figure 4 - (a) HFA Voltage Signal in Droplet Flow; (b) Droplet - Probe Interaction; (c) Voltage Histogram

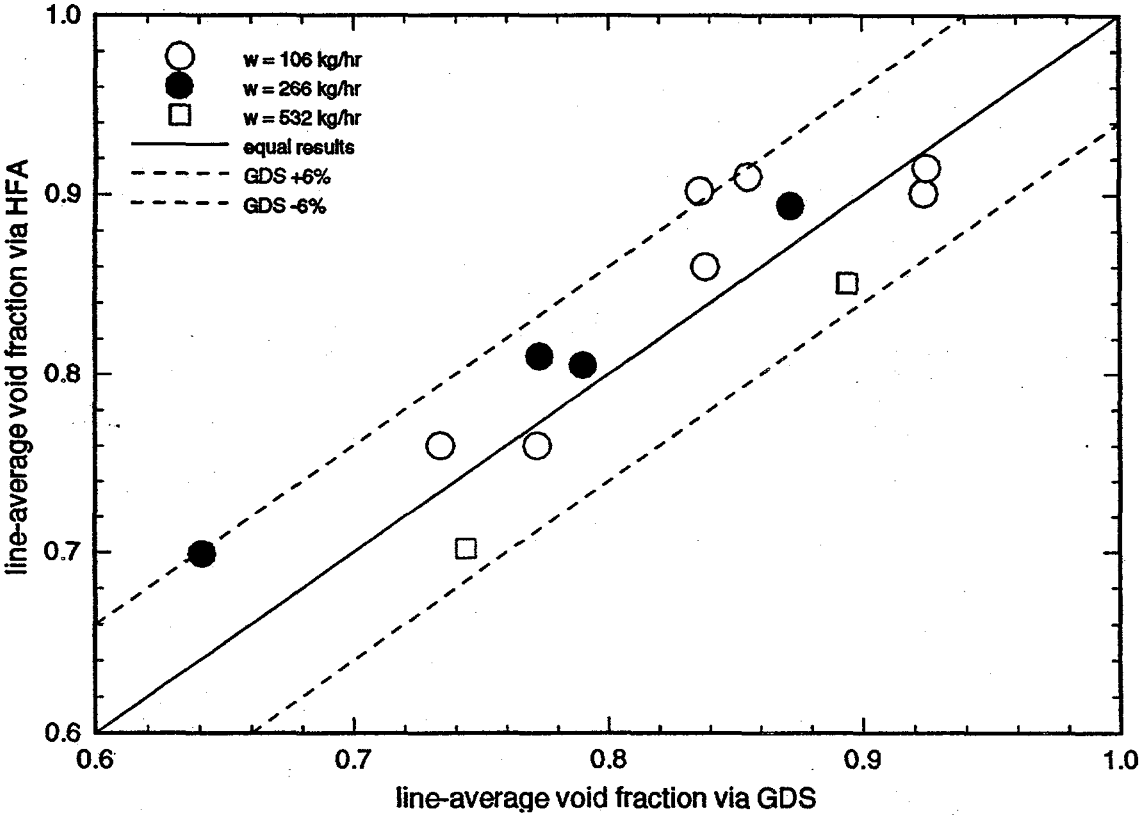

Figure 5 - Comparison of GDS and HFA Void Fraction Results

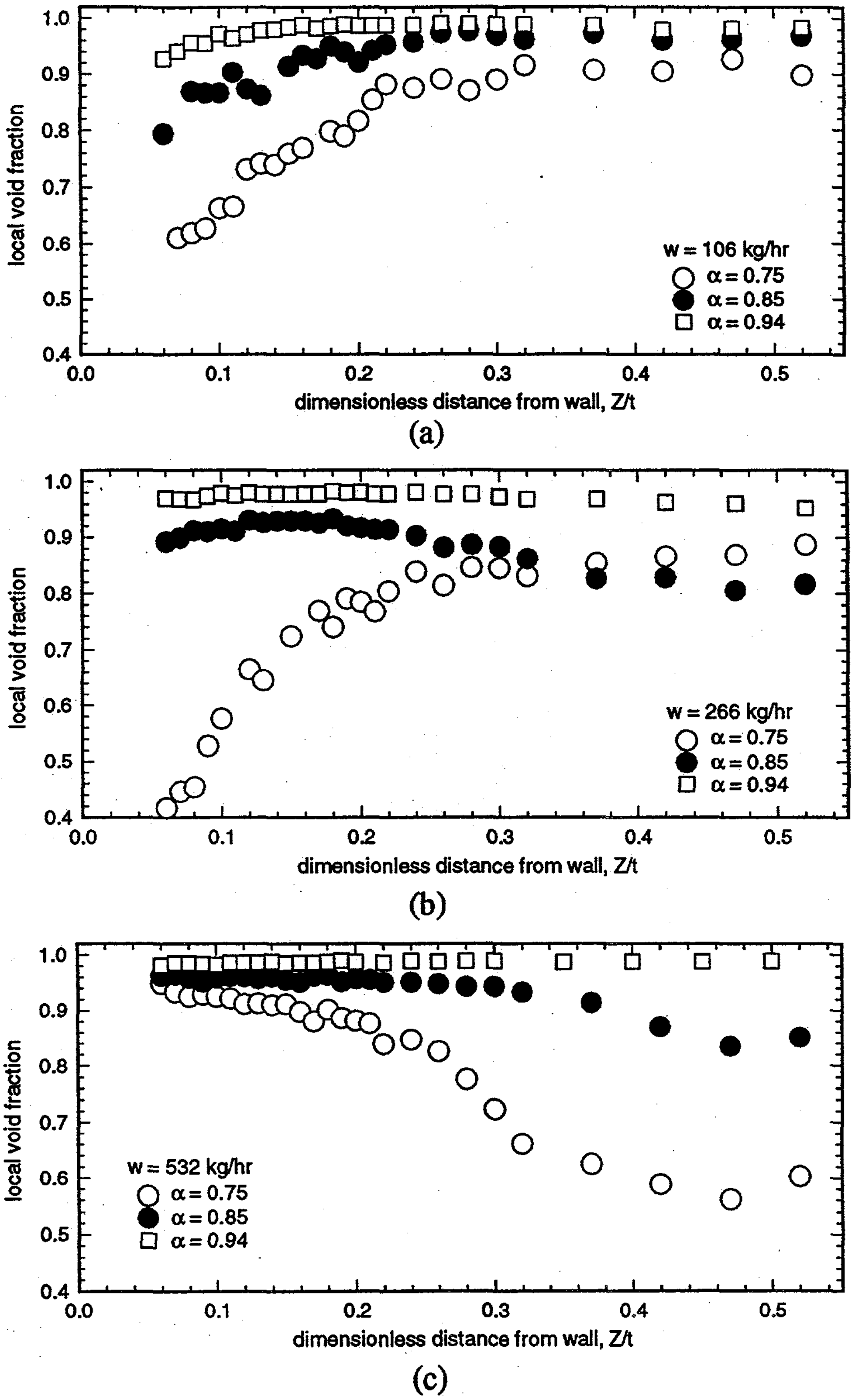

Figure 6 - Void Fraction Profiles for (a) w = 106 kg/hr, (b) 266 kg/hr, and (c) 532 kg/hr

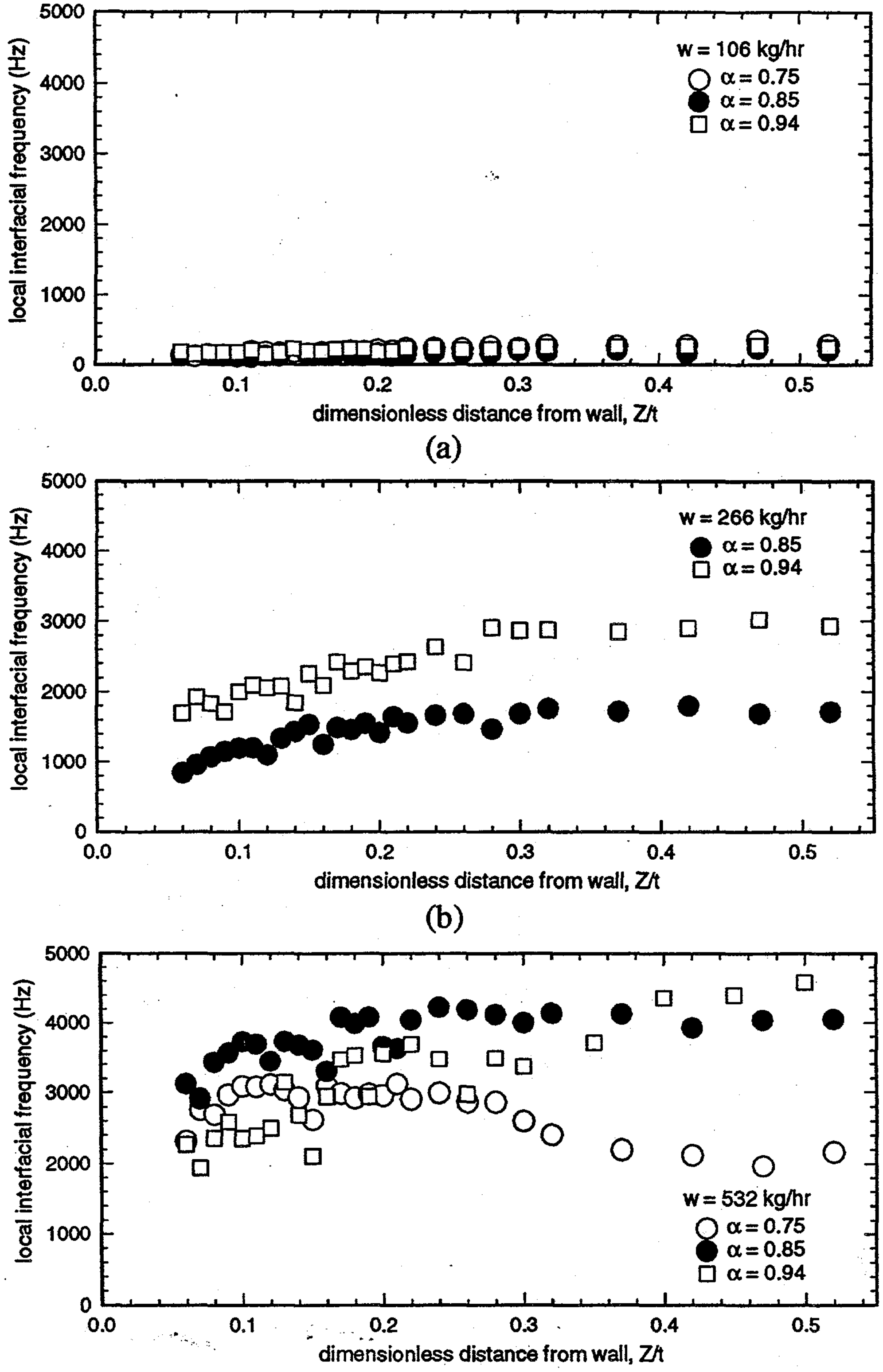

(a)

(b)

(c)

Figure 7 - Interfacial Frequency Profiles for (a) *w* = 106 kg hr, (b) 266 kg/hr, and (c) 532 kg/hr

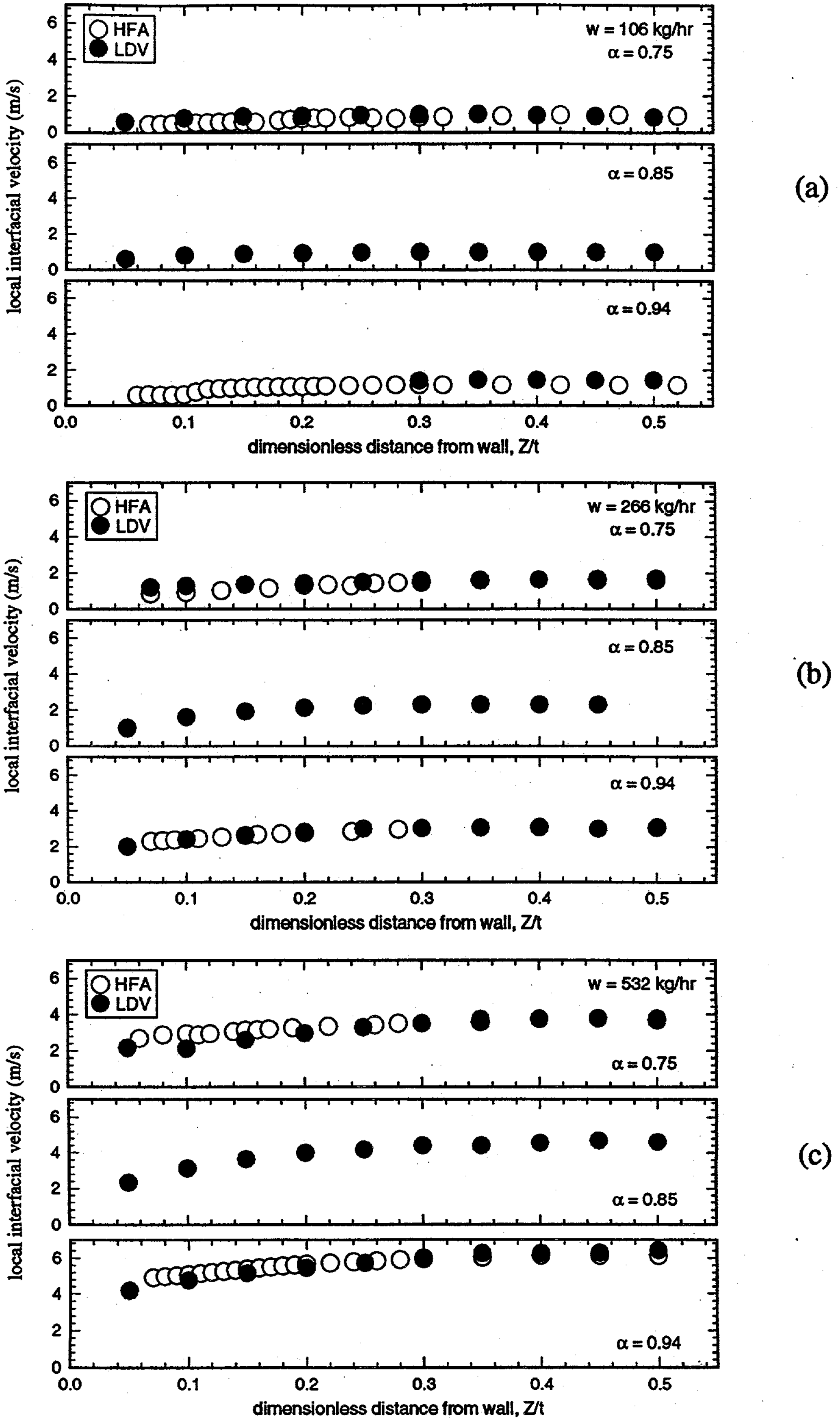

Figure 8 - Interfacial Velocity Profiles for (a) w = 106 kg hr, (b) 266 kg/hr, and (c) 532 kg/hr

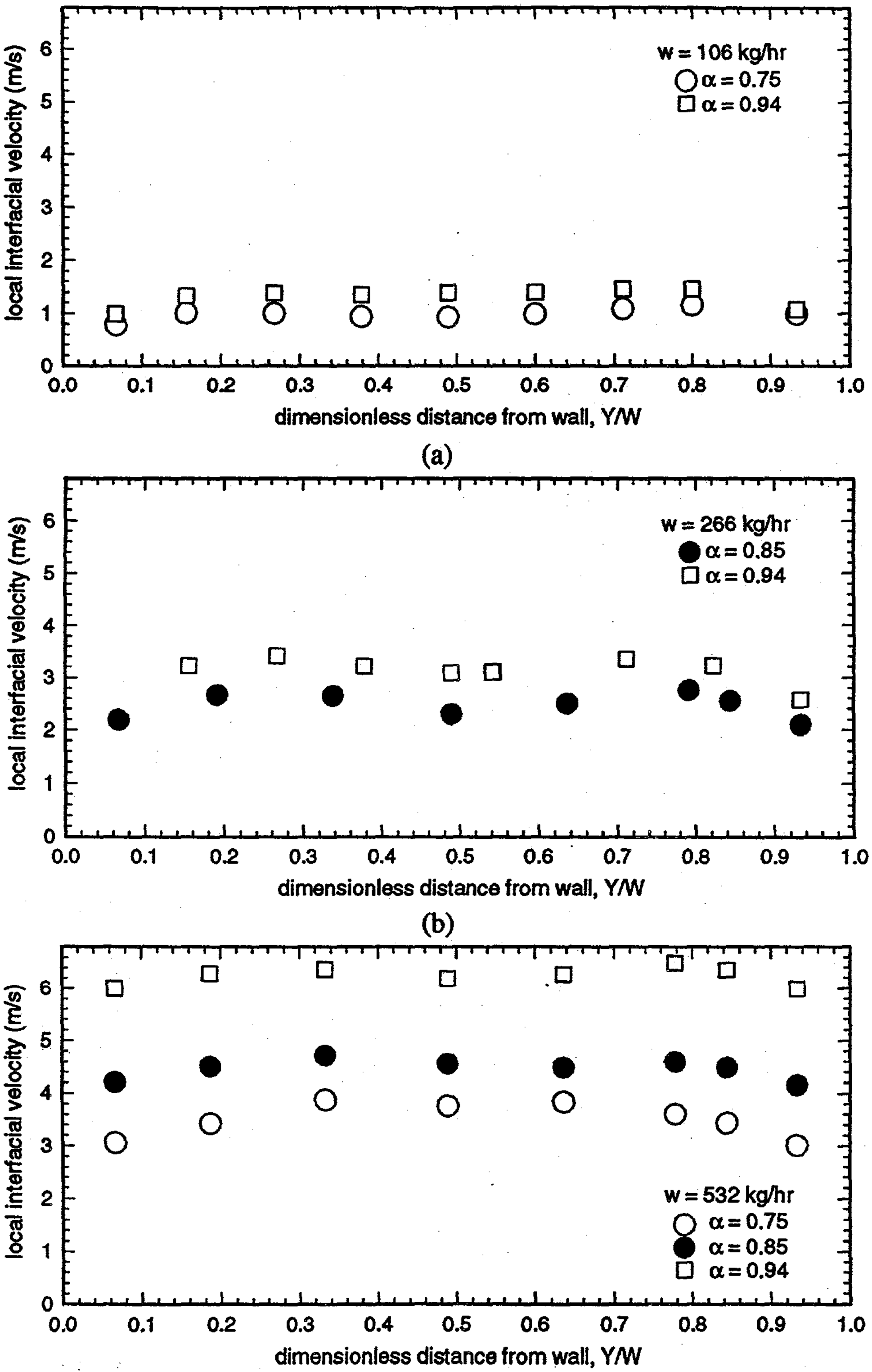

(a)

(b)

(c)

Figure 9 - LDV *Y*-Dimension Interfacial Velocity Profiles for (a) *w* = 106 kg hr, (b) 266 kg/hr, and (c) 532 kg/hr

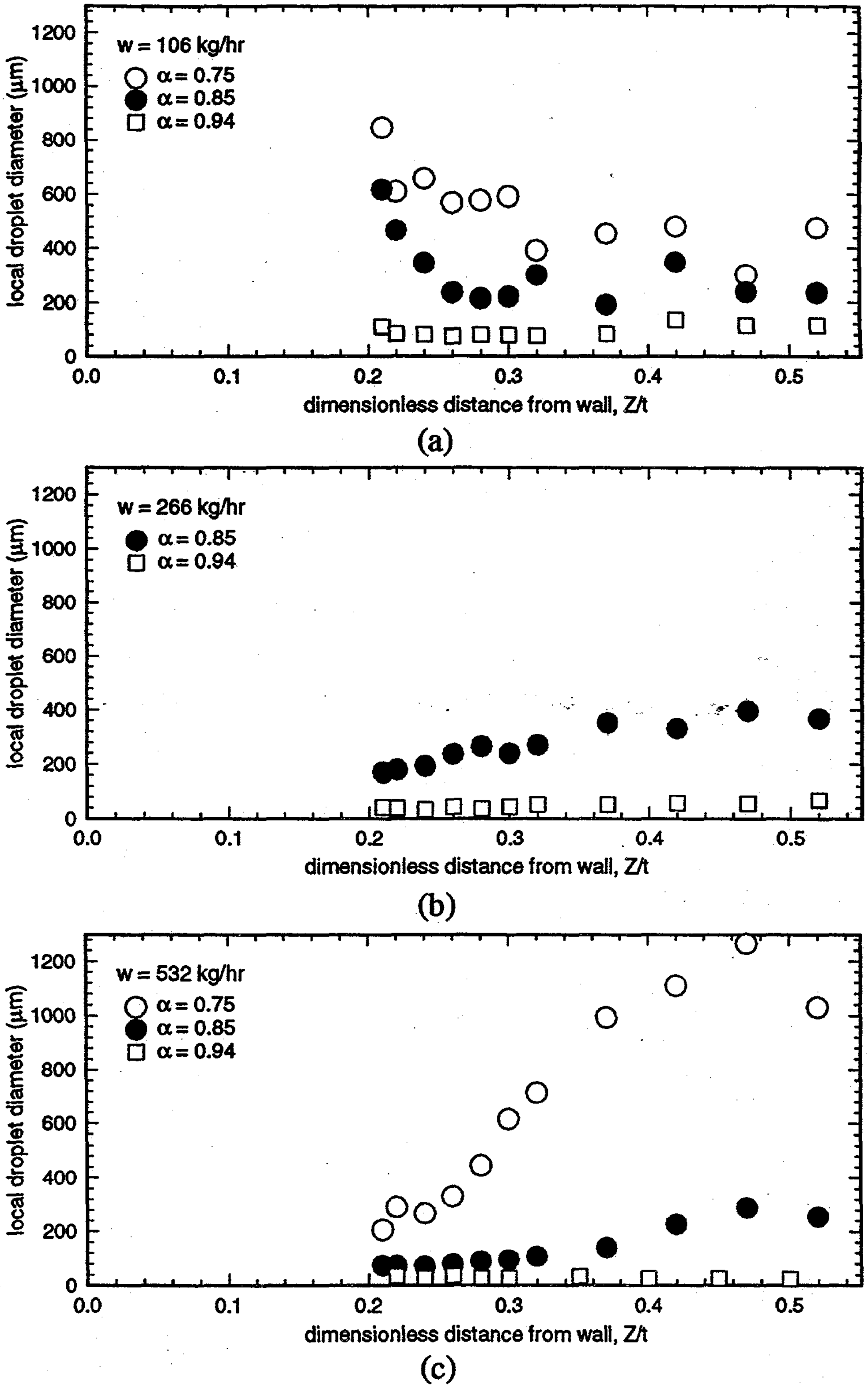

Figure 10 - Droplet Diameter Profiles for (a) *w* = 106 kg hr, (b) 266 kg/hr, and (c) 532 kg/hr

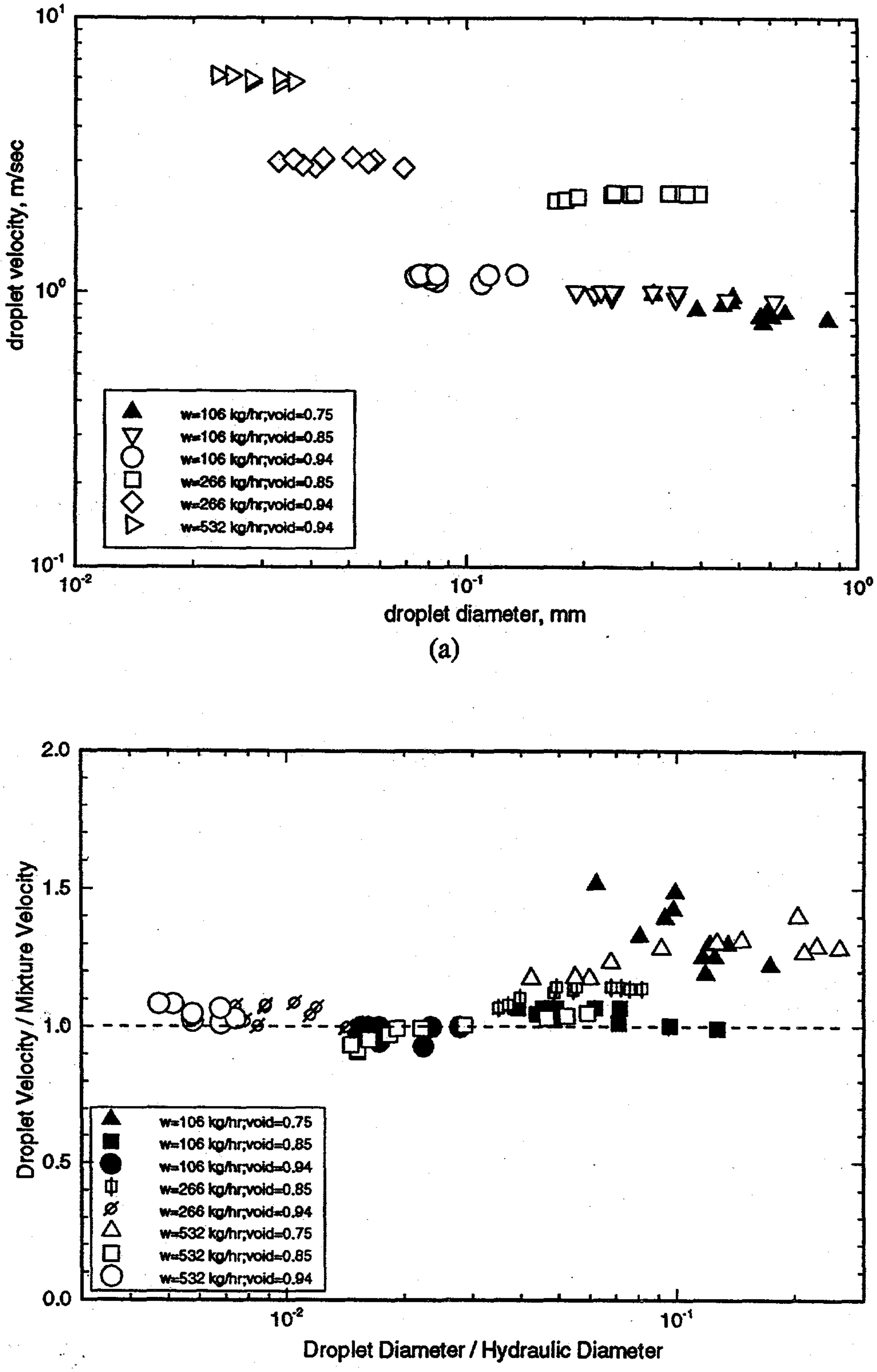

(a)

(b)

Figure 11 - Relationship Between (a) Dimensional and (b) Dimensionless Droplet Size and Velocity

Table 2 - Summary of Mean Droplet Size Experiments

Reference	Fluids	Hydraulic Diameter (mm)	Measurement Technique	We_m	ρ_l/ρ_g	μ_l/μ_g
Wicks and Dukler (1966)	air-water	33.7	electrical conductance	320 - 4100	750	54
Jepson *et al.* (1989)	air-water	10.3	laser diffraction	125 - 1130	555	54
Jepson *et al.* (1989)	helium-water	10.3	laser diffraction	75-218	3700	52
Azzopardi and Teixeira (1994)	air-water	32.0	phase anemometry laser diffraction	220 - 1180	830	57
Fore and Dukler (1995)	air-water	50.8	laser diffraction	240 - 1110	847	57
Fore and Dukler (1995)	air-50% glycerin & water	50.8	laser diffraction	340 - 1050	794	327
present work	R-134a	4.85	hot-film anemometry	94 - 8950	7.3	6.5

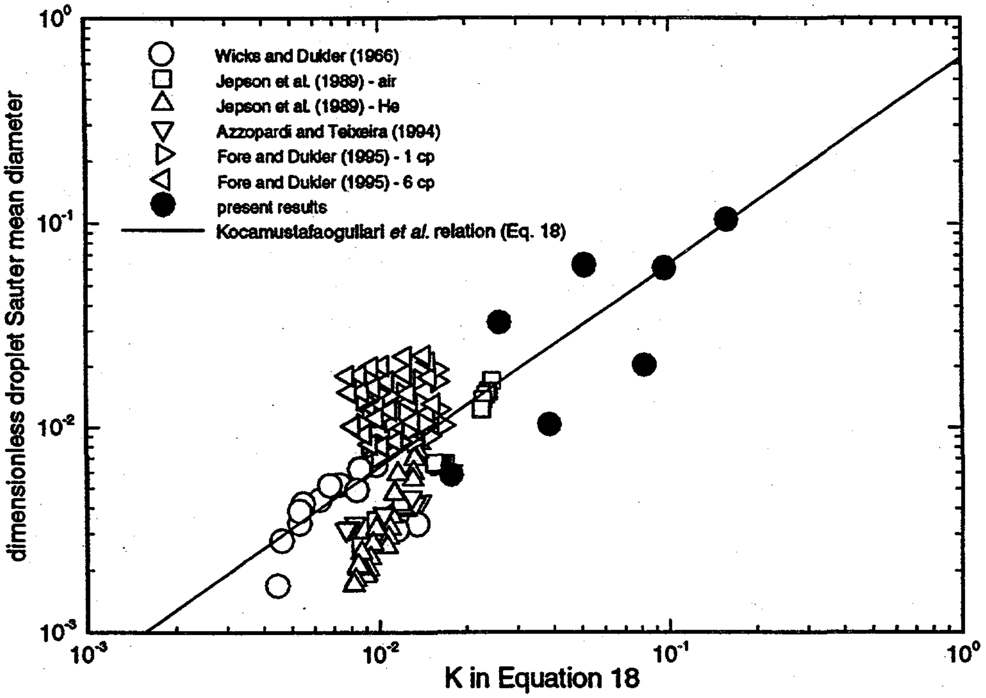

Figure 12 - Comparison of Average Droplet Size Data to Relation of Kocamustafaogullari *et al.* (1994)